GENERAL EXPERIMENTAL
TECHNIQUE

FORMATION OF PULSE-PERIODIC BEAMS OF METAL IONS OF SUBMILLISECOND DURATION WITH HIGH POWER DENSITY

© 2025 A. I. Ryabchikov*, S. V. Dektyarev, A. V. Gurulev

National Research Tomsk Polytechnic University Russia, Tomsk

**e-mail: ralex@tpu.ru*

Received April 27, 2024

Revised August 29, 2024

Accepted September 23, 2024

Abstract. The article presents the results of studies of pulse-periodic formation of aluminum, chromium and titanium ion beams of submillisecond duration based on a source with plasma generation by a continuous vacuum arc discharge. High pulse power density in the ion beam is achieved due to ballistic focusing of ions using a single-electrode grid extractor in the form of a part of a sphere. A method based on the solar eclipse effect is used to clean the ion beam in the area of its crossover from the microdroplet fraction of the vacuum arc plasma. The features and patterns of generation of ion beams of three metals are studied atpulse duration of 450 μs, accelerating voltage up to 40 kV, with a power density in a pulse exceeding 105 W/cm2. It was established that stable formation of pulse-periodic beams of high-intensity metal ions with a submillisecond duration based on vacuum arc plasma is achieved due to ion-electron emission, compensating for the escape of plasma electrons into the accelerating gap.

DOI: 10.31857/S00328162250119e7

1. INTRODUCTION

Pulsed-periodic beams of charged particles and plasma flows, as well as laser radiation of high pulsed power density, find application in scientific research and technologies of modification of properties of various materials and coatings [1–16]. Their modifying effect is based on the peculiarities of pulsed action of energy clots on microstructure and properties of near-surface layers of various materials. Heating during the pulse to high temperatures, sometimes up to melting of the near-surface layer, followed by ultra-fast cooling, due to heat removal into the depth of the material due to thermal conductivity, provides ultra-high hardening rates, not achievable in conventional metallurgy. Powerful energy impact in itself does not provide additional alloying of the material, but can change the microstructure and properties of the near-surface layers due to redistribution of

elements in the impact zone and formation of new phases. A distinctive feature of ion implantation is based on the change in the elemental composition of the near-surface layer with formation of new phases, including due to thermal peaks near ion tracks [17–28].

The limitation of large-scale application of ion implantation for directed improvement of performance properties of metals and alloys is associated with the small range of ions in solid matter. In works [29, 30], it was shown that to increase the thickness of the ion-doped layer, it is necessary to implement a high-current implantation mode with an increase in the ion current density to several milliamperes per square centimeter. This approach was further developed in works [31, 32]. With a relatively low ion energy, usually not exceeding several keV, the ion current density in metal and gas ion beams of microsecond duration was increased to several hundred milliamperes per square centimeter. The increase in ion current density and significant heating of the irradiated target contributed to the enhancement of radiation-stimulated diffusion of implanted atoms. New methods of high-intensity low-energy ion implantation at high average ion beam power have demonstrated the possibility of ion doping of materials at depths of tens and hundreds of micrometers. These methods are effective for ion-diffusion doping of metals and alloys with nitrogen and other elements of the periodic table having a small atomic radius. Their radiation-stimulated diffusion is realized in many cases at low temperatures, when no significant grain growth of the crystalline structure of materials is observed.

The advantages of high-intensity implantation methods in many promising applications are limited by the necessity to heat the entire volume of the product to temperatures at which degradation of the microstructure of metals and alloys occurs due to rapid grain growth. A new method proposing a solution to this problem is presented in reference [33]. The method is based on using high-intensity ion beams with submillisecond pulse duration and power density from several tens to several hundreds of kW/cm ^{2} for deep ion doping of metals. The impact of such an ion beam on the surface leads to its heating during the pulse to high temperatures, up to melting. The high ion current density combined with high temperature promotes a significant increase in the coefficient of radiation-enhanced diffusion. Ultra-rapid cooling of the near-surface layer due to heat transfer into the target provides the possibility of preventing overheating of the material beyond the ion doping region, while simultaneously improving the microstructure of the implanted layer.

The high ion current density, significant pulse duration combined with its frequency should provide a high accumulation rate of ion irradiation fluence necessary for deep ion doping of various materials.

The present work is devoted to studying the features and patterns of formation and diagnostics of metal ion beams, using titanium, chromium, and aluminum ions with submillisecond duration in a source using continuous vacuum arc discharge plasma, achieving pulsed power density in the ion beam of tens and hundreds of kilowatts per square centimeter.

2. ION SOURCE SCHEME AND RESEARCH METHODOLOGY

The studies were conducted using a modified pulse-periodic source of metal ion beams and plasma flows "Raduga 5M" [34]. The scheme of the experimental setup is shown in Fig. 1.

Fig. 1. Experimental Setup Scheme

The experiments were conducted with pulse durations of 450 μs, accelerating voltage amplitudes ranging from 5 kV to 40 kV, and pulse frequencies up to 40 pulses/s. In experiments measuring ion saturation current from vacuum arc plasma, a pulse-periodic generator with pulse durations of 100 μs, pulse frequency of 10^{3} pulses/s, and voltage pulse amplitudes up to 1.8 kV was also used. Plasma generation by vacuum arc discharge was carried out at a residual atmosphere pressure of 10^{-3} Pa in the experimental chamber. The plasma flow was formed by a continuous vacuum arc discharge with arc currents of 130 and 170 A. Instead of a louvre-type plasma filter, a "solar eclipse" system was used for cleaning the plasma from the microdroplet fraction, first proposed in work [35].

To form an ion beam with high pulse power density, a single-electrode focusing system was used, consisting of a grid electrode in the form of a sphere section with a radius of 130 mm and an equipotential space for transporting and focusing the ion beam. In the experiments, a grid electrode with cell dimensions of 1.1×1.25 mm^{2} and 60% transparency was used. A disc electrode, preventing direct flight of microparticles and explosive emission products from the cathode working surface to the beam focusing area, was installed at the center of the focusing electrode. Ion extraction was carried out in a pulse-periodic mode from the free boundary of metallic plasma generated by vacuum arc discharge.

During the experiments, measurements of accelerating voltage and ion beam current were taken. To study the ion current density distribution across the cross-section of the focused ion beam, a sectioned detector with 19 rod-shaped electrodes of 2 mm diameter was used. A photograph of the detector's external appearance is shown in Fig. 2.

Fig. 2. Photograph of the detector with 19 collectors

The ion current pulse of the beam, due to the peculiarities of plasma generation by a vacuum arc discharge, was characterized by significant high-frequency modulation. This made it difficult to estimate the actual current amplitude and its density and, consequently, the achieved power density in the ion beam. To increase the accuracy of current amplitude measurement, averaging of current and voltage pulses was performed over 16 oscillograms using the mathematical apparatus of the Rigol MSO5000 oscilloscope. When using a high-frequency pulse generator, averaging was performed over 1024 pulses.

3. EXPERIMENTAL RESULTS AND DISCUSSION

Experimental studies and numerical modeling of the dynamics of formation of pulsed-periodic titanium ion beams at a pulse frequency of 10^5 pulses/s and bias potential amplitudes up to 2 kV, described in works [35, 36], revealed a problem of limiting the pulse duration due to decompensation of the space charge of the ballistically focused ion beam caused by the escape of plasma electrons into the accelerating gap through the grid structure cells. In further studies, the authors showed the possibility of overcoming the problem of virtual anode formation both by increasing the gas pressure in the experimental chamber and by using an additional thermionic electron source. In work [37], through numerical modeling, it was established that with an increase in ion energy to several tens of keV, stable formation and transportation of a high-current density ion beam can be realized due to a significant increase in ion-electron emission. In the present studies, attention is paid to the formation of ion beams with high power density in a source based on continuous vacuum arc discharge plasma under conditions of increased ion-electron emission.

In order to determine the contribution of ion-electron emission to the total current measured by the collector during the formation of a titanium ion beam, experiments were conducted with a solid collector installed near the end surface of a vacuum arc plasma generator. The collector completely blocked the plasma flow coming from the arc evaporator. Measurements were carried out in a wide range of accelerating voltages from 100 V to 40 kV. Titanium ions in the vacuum arc discharge plasma have an average charge state of about Z =2 [38]. This means that under the experimental conditions, the average ion energy varied from 200 eV to 80 keV. The dependences of the measured current on the accelerating voltage at arc discharge currents of 130 and 170 A are presented in Fig. 3.

Fig. 3. Dependence of the amplitude of the measured current on a stainless steel collector on the average energy of titanium ions at arc discharge currents of 130 and 170 A

In the ion energy range from 200 eV to 1 keV, the amplitude of the measured currents remains constant. These are saturation ion currents from the plasma. When the arc discharge current increases from 130 to 170 A, the saturation ion current from the plasma increases from 1.5 to 3 A. The growth of the ion current by almost a factor of two, disproportionate to the increase in the arc discharge current, is due to the design of the arc evaporator of the "Raduga 5M" ion and plasma source. The arc discharge current passes through the turns of the coil that creates the longitudinal magnetic field. Accordingly, when the arc current increases, the magnitude of the magnetic field also increases, which leads to the focusing of the plasma flow and an increase in the density of the saturation ion current from the plasma. As the ion energy increases from 1 keV to 80 keV, the amplitude of the currents measured by the collector increases to almost 4 A at an arc current of 130 A and to 8.5 A at a discharge current of 170 A. Since the saturation ion current from the plasma should not depend on the amplitude of the accelerating voltage, the current growth is explained by the growth of ion-electron emission from the collector. The current measured by the collector is equal to the sum of the saturation ion current from the plasma and the ion-electron emission current. The data in Fig. 3 provide a basis for constructing the dependence of ion-electron emission coefficients on the amplitude of the accelerating voltage (Fig. 4).

Fig. 4. Dependencies of the ion-electron emission coefficient on ion energy at arc discharge currents of 130 and 170 A

Figure 4 shows that the ion-electron emission coefficient increases from zero to almost two as the ion energy increases from 1 to 80 keV. Increasing the vacuum arc discharge current from 130 to 170 A did not fundamentally change the nature of the dependence of the ion-electron emission coefficient on the average ion energy in the beam.

When forming an ion beam using a grid focusing electrode, ballistic focusing of ions increases the current density by more than two orders of magnitude. During transport of a high-intensity ion beam with different energies in the drift space, its charge neutralization conditions and, consequently, focusing will change. To determine the effect of ion current density on the ion-electron emission coefficient, experiments were conducted with energy measurements in the ion beam. Direct measurements were performed using a thermocouple embedded in a thermally insulated target with a diameter of 15 mm and a thickness of 3 mm. Indirect measurement of the ion beam energy was carried out using averaged oscillograms of the ion current (taking into account the ion-electron emission coefficient), accelerating voltage, pulse frequency, and target irradiation time. To reduce the energy loss accumulated in the sample due to radiation, experiments were conducted with a pulse frequency

in the range of 10–40 pulses/s with a total irradiation time of 20 s. The calorimetric study data provided an estimate of the ion current amplitude approximately 10% lower than when determining energy by the indirect method. This difference may be related to the dynamics of temperature change on the irradiated surface during the ion beam pulse. During the pulse, the surface temperature increased more than 2 times compared to the average temperature measured by the thermocouple. Therefore, radiation losses were caused not only by the sample's radiation with a temperature not exceeding 700 K during the 20 s irradiation time but also by more intense radiation from the surface during its pulse heating to temperatures exceeding 1100 K. Overall, comparison of the obtained data on energy in the ion beam confirmed that increasing the current density in the ion beam during its focusing to values exceeding 1 A/cm ^{2} does not change the ion-electron emission coefficient.

The presence of ion-electron emission plays a dual role. On the one hand, it complicates the evaluation of the ion current and requires determining the overestimation of current and, accordingly, the power density and energy of the ion beam in each specific case of ion irradiation of samples. On the other hand, it is the ion-electron emission that serves as a continuous supplier of electrons, providing compensation for the space charge of the focused ion beam.

The study of the dynamics of spatial focusing of the titanium ion beam was carried out using a system of 19 collectors. The multi-collector system was moved along the axis of the arc evaporator to measure the distribution of the detected current density at different distances. Figure 5 shows the current density distributions in the beam, measured at different distances relative to the geometric focus of the system, with an accelerating voltage of 20 kV and an arc discharge current of 130 A.

Fig. 5. Superposition of distribution profiles of current density detected by collectors across the beam section

The presented data demonstrate the change in the maximum amplitude of the measured current depending on the geometric arrangement of the collectors. Sequential movement of the multi-collector system from the position of -10 mm to +10 mm relative to the geometric focus of the system is accompanied by improved focusing. There is a decrease in FWHM and an increase in the amplitude of the measured current density up to the position F+10 mm. Further displacement to the position F+20 leads to an increase in the measured current density, but with its simultaneous broadening, and in the position F+30, a decrease in the amplitude of the current density is already observed due to defocusing of the ion beam. Increasing the arc discharge current to 170 A led to an increase in the maximum current density, as shown in Fig. 6, by almost two times. The maximum current density along the beam axis reached 3.25 A/cm ^{2}.

Fig. 6. Current density distribution profiles across the beam section

Curve *1* , like most of the data presented in the article, is plotted based on oscilloscope data with amplitude averaging over 16 pulses. It should be noted that in some single pulses, the value of the detected current density exceeded 7.5 A/cm ^{2}, as shown in Fig. 6.

A study of the accelerating voltage influence has shown that as it increases from 8 to 20 kV, the current density along the beam axis increases from 1.5 to 2.25 A/cm ^{2} (Fig. 7). However, further increase in the accelerating voltage amplitude led to a decrease in the maximum current density to 1.9 A/cm ^{2}. The beam half-width changed insignificantly and was about 10 mm.

Fig. 7. Profiles of ion current density distribution across the beam cross-section

Studies on the formation of high-intensity chromium ion beams with high pulse power density showed generally the same patterns and features as in the case of the titanium ion beam. The results of current measurements on a solid collector depending on the ion energy at arc discharge currents of 130 and 170 A are presented in

Fig. 8. As can be seen in the figure, the measured current amplitude changes insignificantly with increasing average ion energy in this range. The value of this current is determined by the ion saturation current from the vacuum arc discharge plasma, and at an arc discharge current of 130 A, under the specific experimental conditions, it was approximately 0.8 A.

Fig. 8. Total current on a solid collector depending on the average energy of chromium ions

When the arc discharge current increases to 170 A, the current amplitude at accelerating voltage in the range from 0.1 to 1.8 kV increases to 2.25 A.

Increasing the accelerating voltage amplitude to 35 kV leads to an increase in the measured current to 1.7 A at an arc current of 130 A and to 5.0 A at an arc discharge with a current of 170 A. Assuming that the increase in the current measured by the collector depending on the accelerating voltage and, accordingly, the ion energy is due to ion-electron emission, the data in Fig. 8 allowed determining the dynamics of changes in the ion-electron emission coefficient. Fig. 9 presents data on changes in ion-electron emission coefficients for a chromium ion beam formed at arc discharge currents of 130 and 170 A.

Fig. 9. Dependence of the ion-electron emission coefficient on ion energy for chromium ion beam

As in the case of titanium ions, changing the arc discharge current does not affect the ion-electron emission value. Moreover, increasing the ion current density during ballistic focusing of

chromium ions also does not affect the ion-electron emission coefficient. Figure 10 demonstrates the dependence of the current registered by the collector of the focused beam on the average ion energy at vacuum arc discharge currents of 130 and 170 A.

Fig. 10. Dependence of the collector current on the average ion energy during ballistic focusing of the chromium ion beam

The collector registers currents lower than those shown in Fig. 8. This decrease is due to ion losses on the grid focusing electrode.

Ion-electron emission provided partial compensation for the escape of plasma electrons into the accelerating gap through the grid electrode cells and, as a result, ensured stable formation of a chromium ion beam with high pulse power density at pulse durations of 450 μs. This means that when forming high-intensity beams with ion energies of several tens of keV, a single-electrode focusing system in the form of a fine-structured grid can also be used to generate a continuous beam with high average power density.

At the same time, unlike the results obtained with the titanium ion beam, when generating a chromium ion beam, both the average over 16 pulses and in individual pulses, the maximum power density was almost two times lower. This may be due to a lower ion-electron emission coefficient. Reducing the number of electrons generated as a result of ion-electron emission changes the degree of neutralization of the ion beam space charge. As a consequence, ion focusing conditions deteriorate. When forming a titanium ion beam, incomplete compensation of the ion beam space charge also took place. This is evidenced by data on the displacement of the beam crossover beyond the geometric focus of the focusing system.

The data on changes in the current amplitude on a solid collector versus the average energy of aluminum ions at vacuum arc discharge currents of 130 and 170 A are presented in Fig. 11.

Fig. 11. Dependence of the collector current amplitude on the average energy of aluminum ions

At a discharge current of 170 A, the ion saturation current from aluminum plasma, measured at voltage amplitudes not exceeding 1 kV, is approximately 3 A. When the accelerating voltage increases to 40 kV and, accordingly, the average ion energy, taking into account the average charge state of ions Z =1.72 [38], increases to approximately 70 keV, the collector current increases due to ion-electron emission to 7.8 A. The dependence of the ion-electron emission coefficient on the energy of aluminum ions is shown in Fig. 12.

Fig. 12. Dependence of the ion-electron emission coefficient on ion energy for an aluminum ion beam

At the maximum ion energy, the ion-electron emission coefficient approaches 1.6. As in the cases with titanium and chromium ion beams, the dependence of the ion-electron emission coefficient does not depend on the ion current density in the range from a few units to hundreds of mA/cm ^{2}. Throughout the entire range of accelerating voltages, the ion beam was stable without showing instabilities associated with the decompensation of its space charge.

4. CONCLUSION

As a result of comprehensive studies of the features and patterns of formation, focusing, and diagnostics of pulsed ion beams with high pulse power density at accelerating voltages up to 40 kV, with average ion energy considering their charge state up to 80 keV, it has been established that submillisecond-duration beams of titanium, chromium, and aluminum ions are stable, efficiently transported, and focused throughout the pulse duration of up to 450 μs. It is shown that, unlike the case of metal ion beam formation at low accelerating voltages, when the emergence of a virtual anode leads to a breakdown in ion beam transport, increasing the ion energy leads to ion-electron emission, which improves the neutralization of the beam space charge and compensates for the escape of electrons into the accelerating gap through the grid electrode elements. It has been established that the change in the ion-electron emission coefficient with ion energy does not depend on the ion current density in a wide range from several units to several hundred mA/cm ^{2}, but is determined by the type of ions. The maximum ion-electron emission coefficient at an accelerating voltage of 40 kV was 2 for titanium ions, 1.3 for chromium ions, and 1.6 for aluminum ions. Using the titanium ion beam as an example, it is shown that as a result of incomplete neutralization of the ion beam space charge, its crossover is displaced by 20 mm beyond the geometric focus of the system. The maximum power density for the titanium ion beam averaged over 16 pulses approached 110 kW/cm ^{2}, and in individual pulses exceeded 200 kW/cm ^{2}. Slightly lower power densities were obtained for aluminum and chromium ion beams.

Ion beams with such parameters are undoubtedly attractive for implementing the method of deep ion doping of materials, based on the synergy of high-intensity implantation with simultaneous energy impact of the ion beam on the surface of the irradiated target.

FUNDING

The study was supported by the Russian Science Foundation (project No. 22-19-00051). (https://rscf.ru/project/22-19-00051/)

REFERENCES

1. *Shulov V.A., Paikin A.G., Teryaev D.A., Bytsenko O.A., Engel'ko V.I., Tkachenko K.I.* // Inorganic Materials: Applied Research. 2013. V. 4. P. 189. http://doi.org/10.1134/S2075113313030118

2. *Koval B.A., Mesyats G.A., Ozur G.E., Proskurovsky D.I., Yankelevich E.B.* High-current pulsed electron beams in technology. Collection. / Ed. G.A. Mesyats. Novosibirsk: Nauka, 1983.

3. *Ozur G.E., Proskurovsky D.I.* // Plasma Phys. Rep. 2018. V. 44. P. 18. http://doi.org/10.1134/S1063780X18010130

4. *Vorobyov M.S., Teresov A.D., Moskvin P.V., Koval N.N., Doroshkevich S.Y., Shin V.I.* // 7th International Congress on Energy Fluxes and Radiation Effects (EFRE), Tomsk, Russia, 2020. P. 492. http://doi.org/10.1109/EFRE47760.2020.9241895

5. *Kaikanov M., Kozlovskiy A., Abduvalov A., Dukenbayev K., Zdorovets M.V., Tikhonov A.* // J Mater Sci: Mater. Electron. 2019. V. 30. P. 15724. http://doi.org/10.1007/s10854-019-01958-x

6. *Kuang X., Li L., Wang L., Li G., Huang K., Xu Y.*, // Surf. Coatings Technol. 2019. V. 374. P. 72. http://doi.org/10.1016/j.surfcoat.2019.05.055

7. *Ryabchikov A.I., Dektyarev S.V., Korneva O.S., Lopatin I.V., Sivin D.O.*, *Ivanov Y.F.,* // 7th International Congress on Energy Fluxes and Radiation Effects (EFRE). 2020. P. 702. http://doi.org/10.1109/EFRE47760.2020.9242058 .

8. *Rej D.J., Davis H.A., Olson J.C., Remnev G.E., Zakoutaev A.N., Ryzhkov V.A., Strurs V.K., Isakov I.F., Shulov V.A., Nochevnaya N.A., Stinnett R.W., Neau E.L., Yatsui K., Jiang W.* // J. Vac. Sci. Technol. A. 1997. V. 15. P. 1089. http://doi.org/10.1116/1.580435

9. *Shulov V.A., Nochovnaya N.A., Remnev G.E., Pellerin F., Monge-Cadet P.* // Surf. Coat. Technol. 1998. V. 99. P. 74. http://doi.org/10.1016/S0257-8972(97)00408-8

10. *Bandura N., Byrka O.V., Chebotarev V.V., Garkusha I.E., Makhlaj V.A., Medvedev V., Taran V.S., Tereshin V.I., Skoblo T.S., Pugach S.G.* // Intern. J. Plasma Environ. Sci. Technol. 2011. V. 5. P. 2. http://doi.org/10.34343/ijpest.2011.05.01.002

11. *Garkusha I.E., Byrka O.V., Chebotarev V.V., Derepovski N.T., Müller G., Schumacher G., Poltavtsev N.S., Tereshin V.I.* // Vacuum. 2000. V. 58. P. 195. http://doi.org/10.1016/S0042-207X(00)00168-8

12. *Uglov V.V., Cherenda N.N., Anishchik V.M., Stalmashonak A.K., Astashinski V.M., Mishchuk A.A.* // Vacuum. 2007. V. 81. P. 1341. http://doi.org/10.1016/j.vacuum.2007.01.041

13. *Poate J.M., Foti G., Jacobson D.C.* Surface Modification and Alloying by Laser, Ion, and Electron Beams. Berlin: Springer, 2013.

14. *Wang D., Yang Y., Guo T., Xiong X., Xie Y., Li K., Li B., Ghali M.* // Sol. Energy. 2021. V. 213. P. 118. https://doi.org/10.1016/j.solener.2020.11.041

15. *Huang J.* // Optik. 2021. V. 226. P. 165437. https://doi.org/10.1016/j.ijleo.2020.165437

16. *Li Y., Wu Y., Wang W., Lei M., Li X.* // Surf. Coat. Technol. 2021. V. 405. P. 126567. https://doi.org/10.1016/j.surfcoat.2020.126567

17. *Williams J. S., Poate J.M.* Ion Implantation and Beam Processing. Orlando: Academic, 1984.

18. *Wang F., Khan A., Ayaz M., Ahmad I., Nawaz R., Gul N.* // J. Math. 2020. V. 2020. P. 8875976. https://doi.org/10.1155/2020/8875976

19. *Anders A.*, Handbook of Plasma Immersion Implantation and Deposition. New York: John Wiley & Sons, 2000.

20. *Komarov F.F., Yuvchenko, V.N. //* Tech. Phys. 2003. V. 48. P. 717. https://doi.org/10.1134/1.1583824

21. *Belyi A.V., Kukareko V.A., Lobodaeva O.V.* Ion-beam treatment of metals, alloys and ceramic materials. Minsk: Belarus. navuka, 1998.

22. *Kozlov E.V., Ryabchikov A.I., Sharkeev Yu.P., Stepanov I.B., Fortuna S.V., Sivin D.O., Kurzina I.A., Prokopova T.S., Mel'nik I.A. //* Surf. Coat. Technol. 2002. V. 158. P. 343. https://doi.org/10.1016/S0257-8972(02)00275-X

23. *Moncoffre N., Jagielski J.* // Surf. Coat. Technol. 1994. V. 65. P. 30. https://doi.org/10.1016/S0257-8972(94)80005-7

24. *Shipilova O.I., Gorbunov , V.L. Paperny S.P., Chernykh A.A., Dresvyansky V.P., Martynovich E.F., Rakevich A.L.* // Surf. Coat. Technol. 2020. V. 393. P. 125742. https://doi.org/10.1016/j.surfcoat.2020.125742

25. *Zatsepin D.A., Boukhvalov D.W., Zatsepin A.F., Mikhaylov A.N., Gerasimenko N.N., Zaporochan O.A.* // J. Mater Sci. 2021. V. 56. P. 2103.

https://doi.org/10.1007/s10853-020-05319-6

26. *Hutchings R.* // Mater. Sci. Eng. A. 1994. V. 184. P. 87.

https://doi.org/10.1016/0921-5093(94)91023-5

27. *Zhang L.C., Chen L.Y., Wang L.* // Adv. Eng. Mater. 2020. V. 5. P. 1901258. https://doi.org/10.1002/adem.201901258

28. *Pelletier J., Anders A.* // IEEE Transactions on Plasma Science. 2005. V. 33. P. 1944. https://doi.org/10.1109/TPS.2005.860079

29. *Wei R.* // Surf. Coat. Technol. 1996. V. 83. P. 218.

https://doi.org/10.1016/0257-8972(95)02828-5

30. *Wilbur P. J., Davis J. A., Wei R., Vajo J.J., Williamson D.L. //* Surf. Coat. Technol. 1996. V. 83. P. 250. https://doi.org/10.1016/0257-8972(95)02830-7

31. *Ryabchikov A.I., Sivin D.O., Ananin P.S., Ivanova A.I., Lopatin I.V., Korneva O.S., Shevelev A.E.* // Surf. Coat. Technol. 2018. V. 355. P. 129. https://doi.org/10.1016/j.surfcoat.2018.02.110

32. *Ryabchikov A.I., Kashkarov E.B., Shevelev A.E., Obrosov A., Sivin D.O.* // Surf. Coat. Technol. 2019. V. 372. P. 1. https://doi.org/10.1016/j.surfcoat.2019.05.020

33. *Ryabchikov A.I.* // IEEE Trans. Plasma Sci. 2021. V. 49. P. 2529. https://doi.org/10.1109/TPS.2021.3073942

34. *Ryabchikov A.I., Ryabchikov I.A., Stepanov I.B., Dektyarev S.V.* // Rev. Sci. Instrum. 2006. V. 77. P. 03B516. https://doi.org/10.1063/1.2171674

35. *Ryabchikov A.I., Ananin P.S., Dektyarev S.V, Sivin D.O., Shevelev A.E.* // Vacuum. 2017. V. 143. P. 447. https://doi.org/10.1016/j.vacuum.2017.03.011

36. *Koval T. V., Ryabchikov A. I., An T. M. K., Shevelev A. R., Sivin D. O., Ivanova A. I., Paltsev D. M.* // Journal of Physics: Conference Series. 2018. V. 1115. P. 032007. https://doi.org/10.1088/1742-6596/1115/3/032007

37. *Ryabchikov A.I., Tarakanov V.P., Korneva O.S., Sivin D.O., Gurulev A.V.* // Nuclear Instruments and Methods in Physics Research, Section B: Beam Interactions with Materials and Atoms. 2022. V. 533. P. 29. https://doi.org/10.1016/j.nimb.2022.10.015

38. *Brown I.G., Godechot X.* // IEEE Transactions on Plasma Science. 1991. V. 19. P. 713. https://doi.org/10.1109/27.108403

FIGURE CAPTIONS

Fig. 1. Experimental setup diagram: *1* – vacuum arc plasma generator, *2* – electrode for microparticle cutoff, *3* – pulse pyrometer, *4* – grid focusing electrode, *5* – vacuum chamber, *6* – thermocouple, *7* – collector, *8* – pulse-periodic generator of high-voltage pulses with positive polarity.

Fig. 2. Photo of the detector with 19 collectors.

Fig. 3. Dependence of the measured current amplitude on the stainless steel collector on the average energy of titanium ions at arc discharge currents of 130 and 170 A.

Fig. 4. Dependencies of the ion-electron emission coefficient on ion energy at arc discharge currents of 130 and 170 A.

Fig. 5. Superposition of density distribution profiles of current registered by collectors across the beam cross-section, measured at different distances relative to the geometric focus of the ballistic focusing system at an arc discharge current of 130 A and accelerating voltage of 20 kV.

Fig. 6. Profiles of current density distribution across the beam cross-section at arc discharge currents of 130 and 170 A at a distance of F+20 mm, with accelerating voltage of 20 kV.

Fig. 7. Profiles of ion current density distribution across the beam cross-section at an arc discharge current of 130 A at a distance of F+20 mm and different accelerating voltage amplitudes.

Fig. 8. Total current on the solid collector depending on the average energy of chromium ions at vacuum arc discharge currents of 130 and 170 A.

Fig. 9. Dependence of the ion-electron emission coefficient on ion energy for a chromium ion beam at vacuum arc discharge currents of 130 and 170 A.

Fig. 10. Dependence of the collector current on the average ion energy during ballistic focusing of a chromium ion beam formed from vacuum arc plasma at discharge currents of 130 and 170 A.

Fig. 11. Dependence of the collector current amplitude on the average energy of aluminum ions at arc discharge currents of 130 and 170 A.

Fig. 12. Dependence of the ion-electron emission coefficient on ion energy for an aluminum ion beam at vacuum-arc discharge currents of 130 and 170 A.

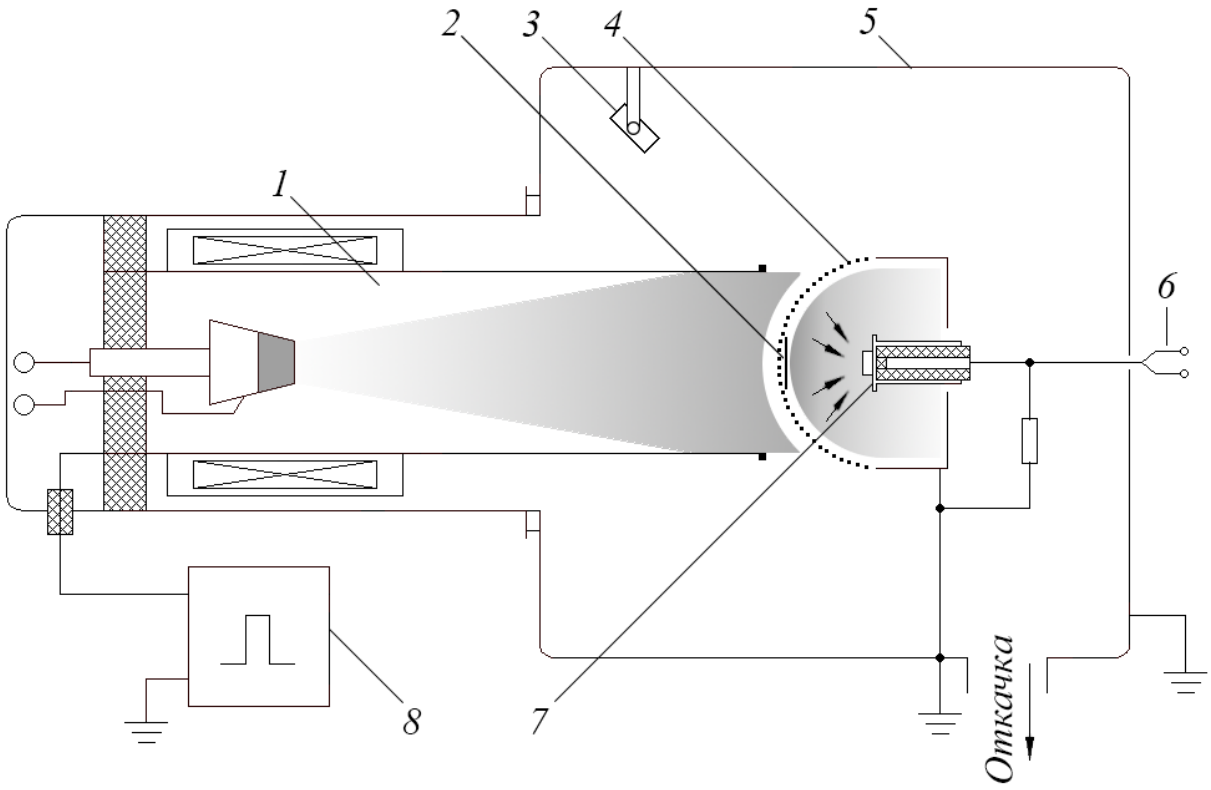

Fig. 1.

Fig. 2.

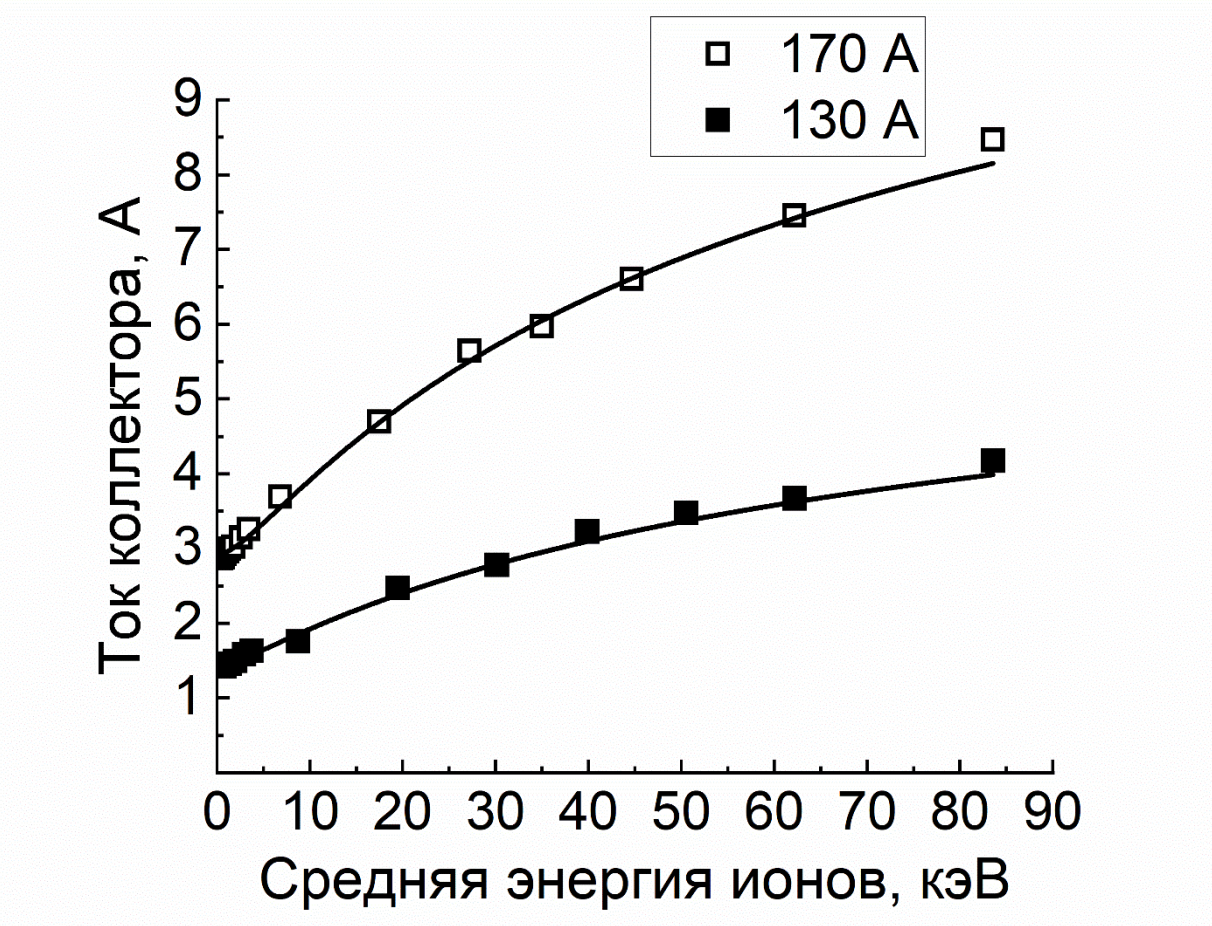
170 A
130 A
Ток коллектора, А
Средняя энергия ионов, кэВ
1
2
3
4
5
6
7
8
9
0
10
20
30
40
50
60
70
80
90

Fig. 3.

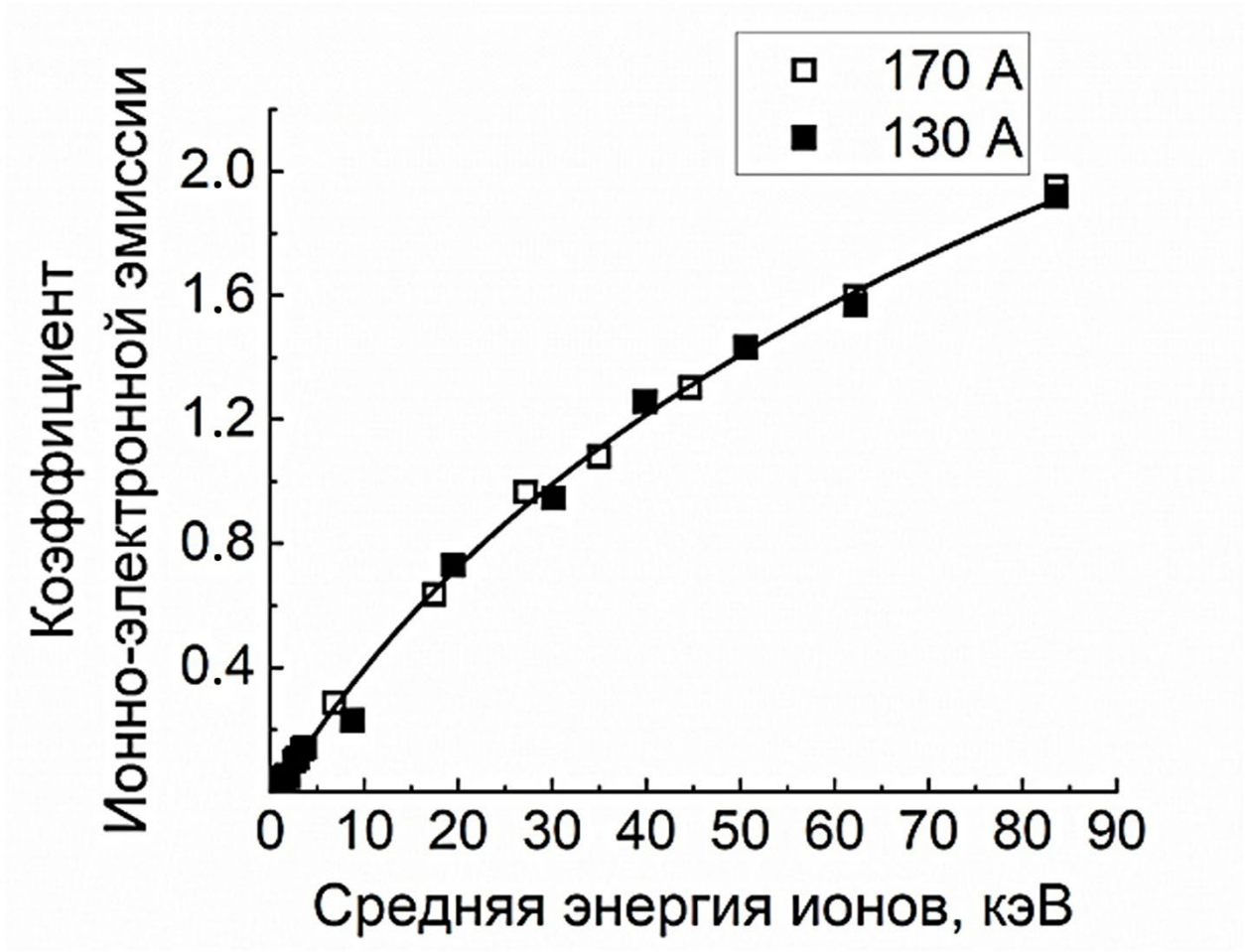
170 A
130 A
Коэффициент
Ионно-электронной эмиссии
2.0
1.6
1.2
0.8
0.4
0
10
20
30
40
50
60
70
80
90
Средняя энергия ионов, кэВ

Fig. 4.

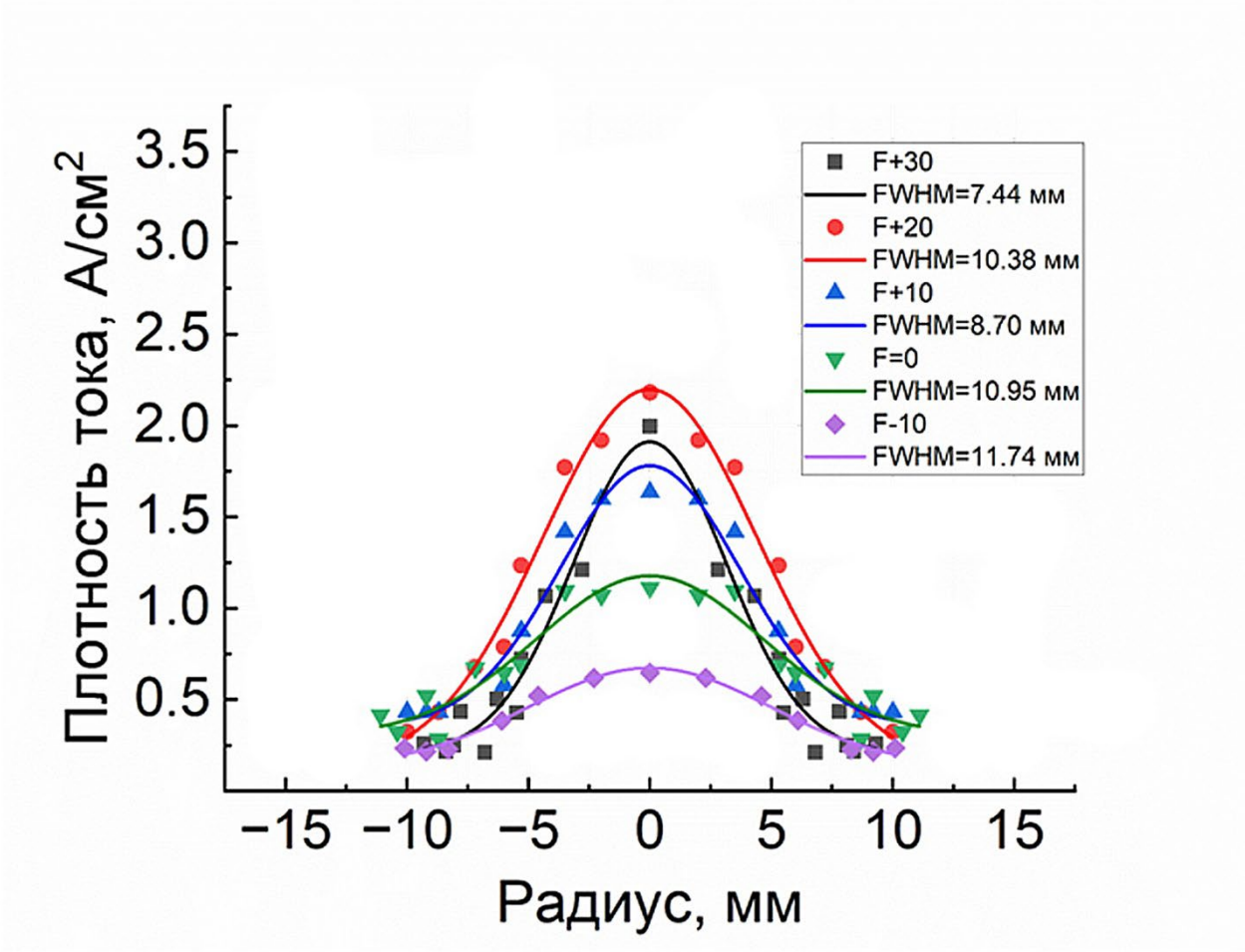
Плотность тока, А/см^2
3.5
3.0
2.5
2.0
1.5
1.0
0.5
−15
−10
−5
0
5
10
15
Радиус, мм
F+30
FWHM=7.44 мм
F+20
FWHM=10.38 мм
F+10
FWHM=8.70 мм
F=0
FWHM=10.95 мм
F-10
FWHM=11.74 мм

Fig. 5.

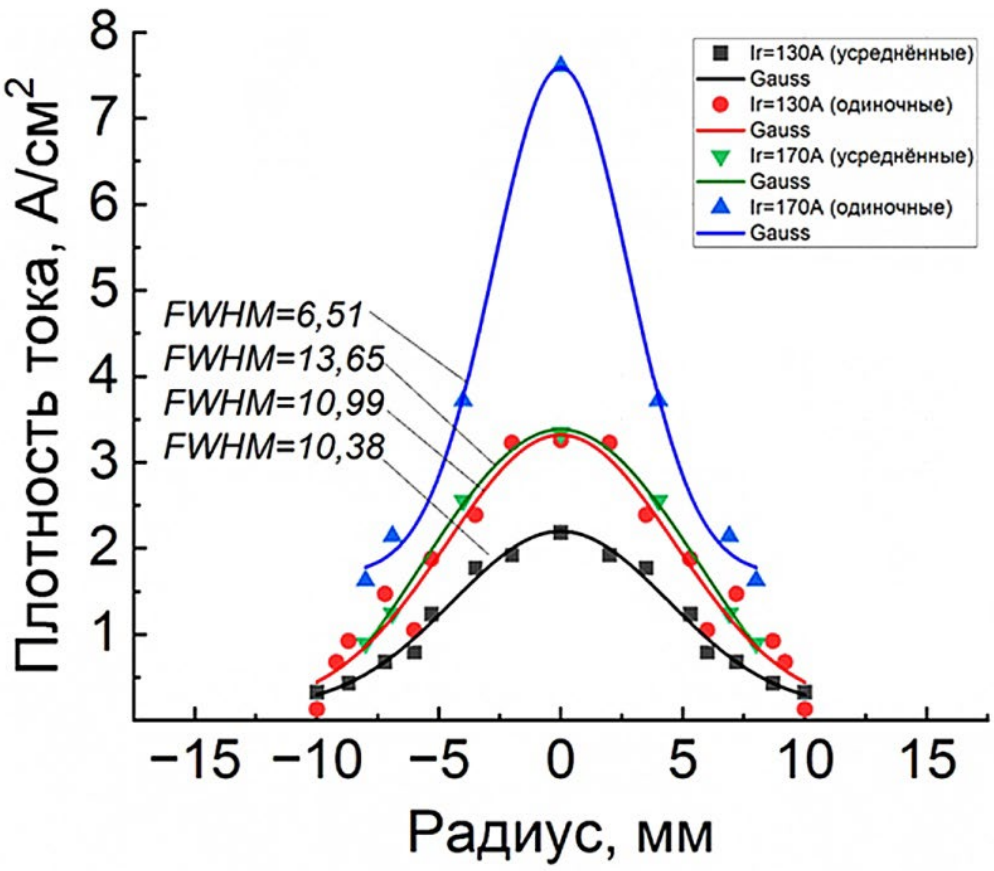
Ir=130A (усреднённые)
Gauss
Ir=130A (одиночные)
Gauss
Ir=170A (усреднённые)
Gauss
Ir=170A (одиночные)
Gauss
FWHM=6,51
FWHM=13,65
FWHM=10,99
FWHM=10,38
Плотность тока, А/см2
Радиус, мм
8
7
6
5
4
3
2
1
−15
−10
−5
0
5
10
15

Fig. 6.

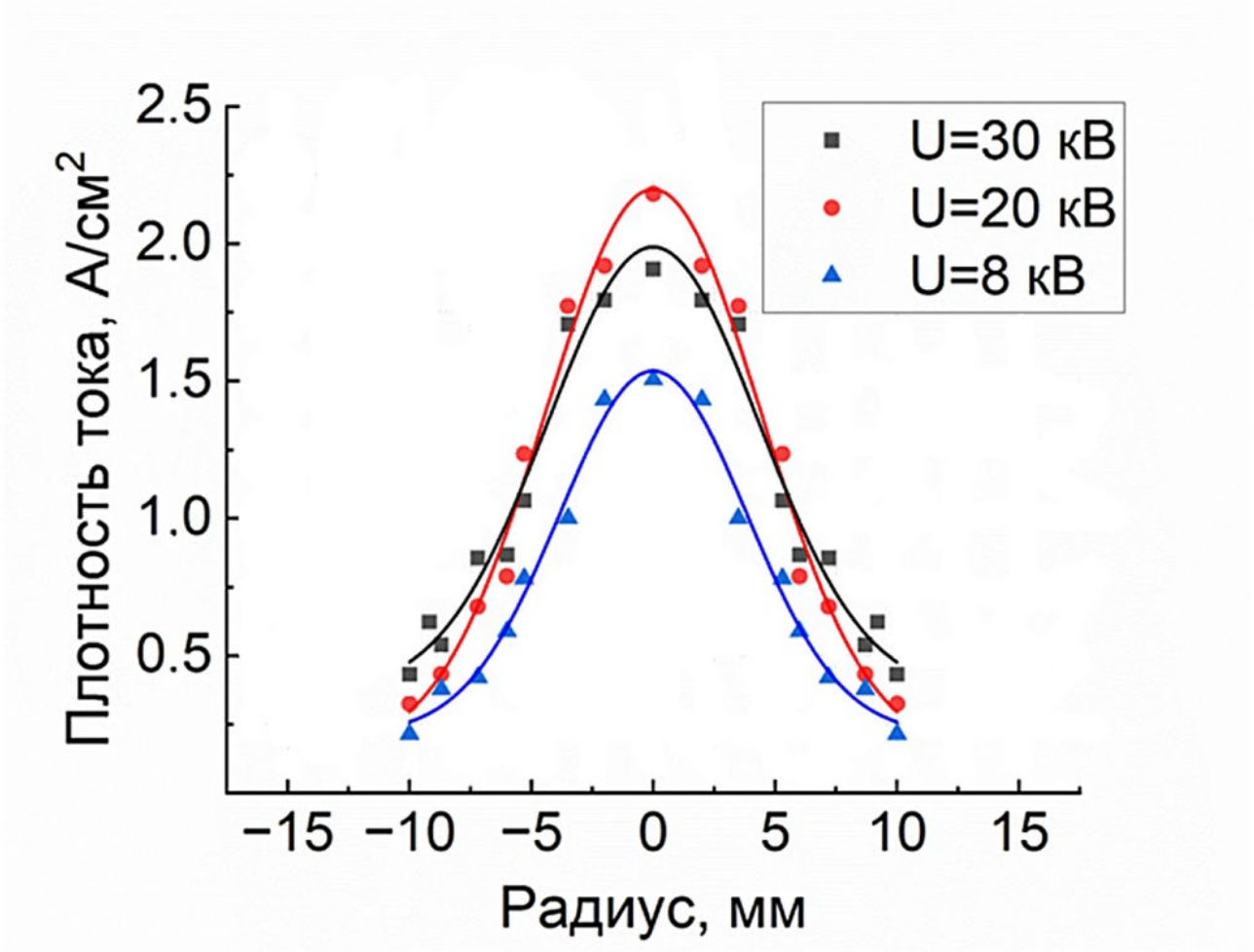
Плотность тока, А/см²
2.5
2.0
1.5
1.0
0.5
−15
−10
−5
0
5
10
15
Радиус, мм
U=30 кВ
U=20 кВ
U=8 кВ

Fig. 7.

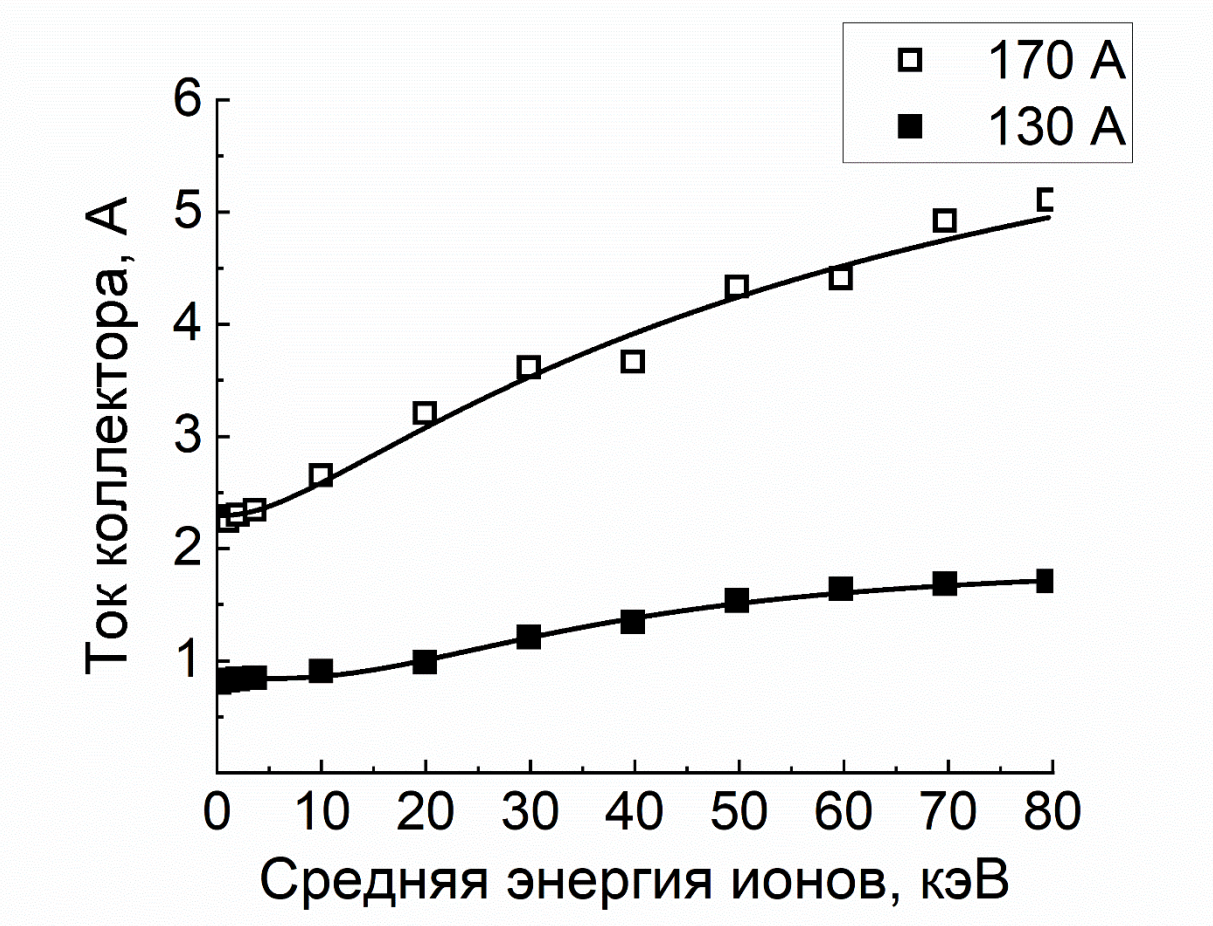
170 A
130 A
Ток коллектора, А
Средняя энергия ионов, кэВ
1
2
3
4
5
6
0
10
20
30
40
50
60
70
80

Fig. 8.

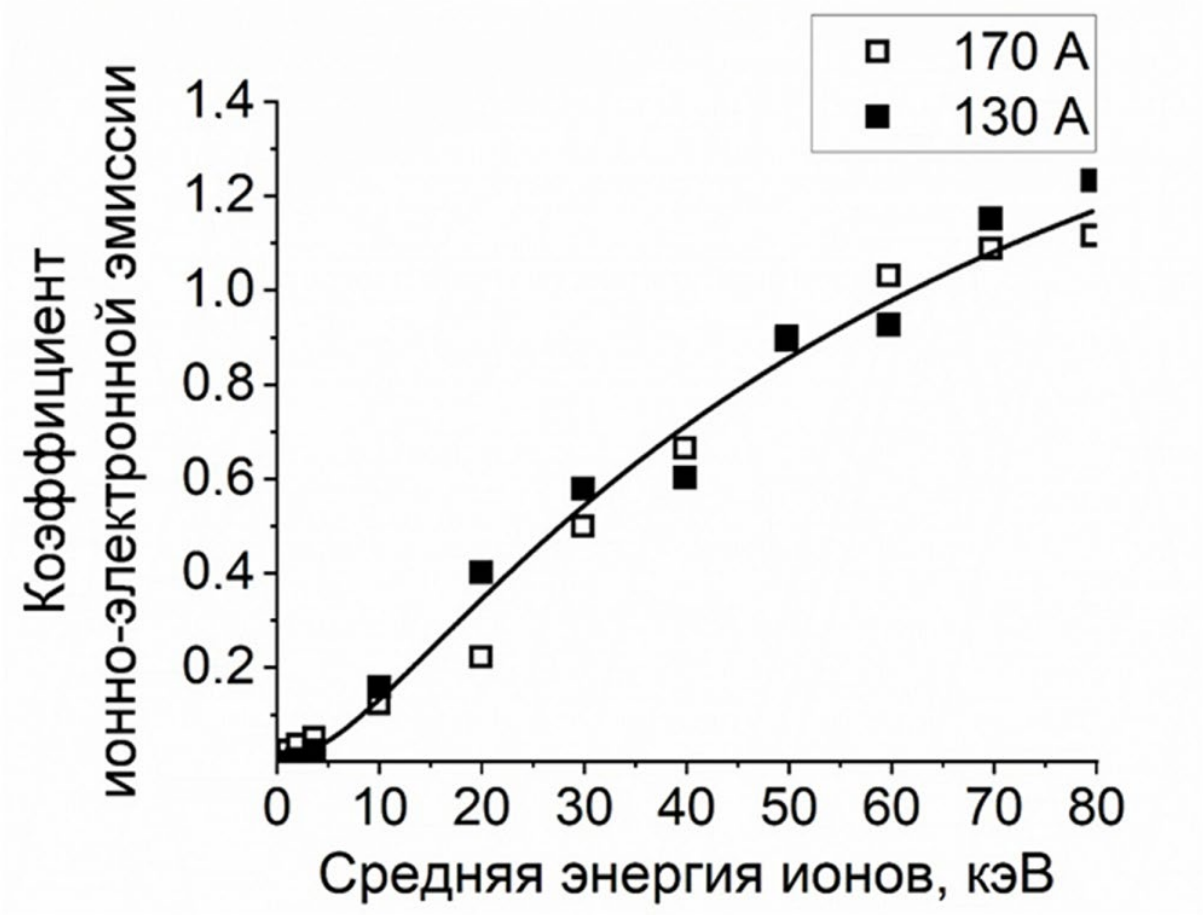
170 A
130 A
Коэффициент ионно-электронной эмиссии
1.4
1.2
1.0
0.8
0.6
0.4
0.2
0
10
20
30
40
50
60
70
80
Средняя энергия ионов, кэВ

Fig. 9.

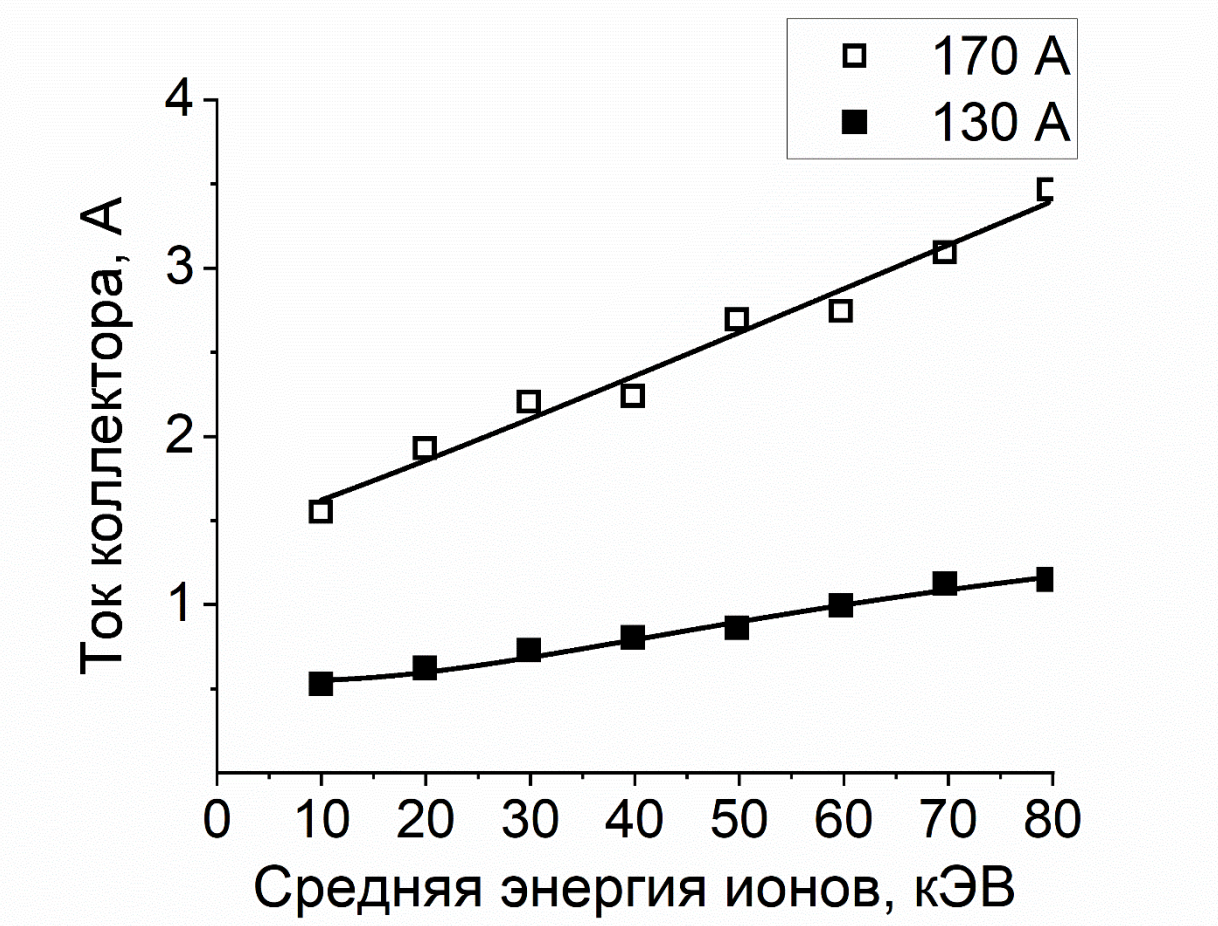
170 A
130 A
Ток коллектора, А
4
3
2
1
0
10
20
30
40
50
60
70
80
Средняя энергия ионов, кЭВ

Fig. 10.

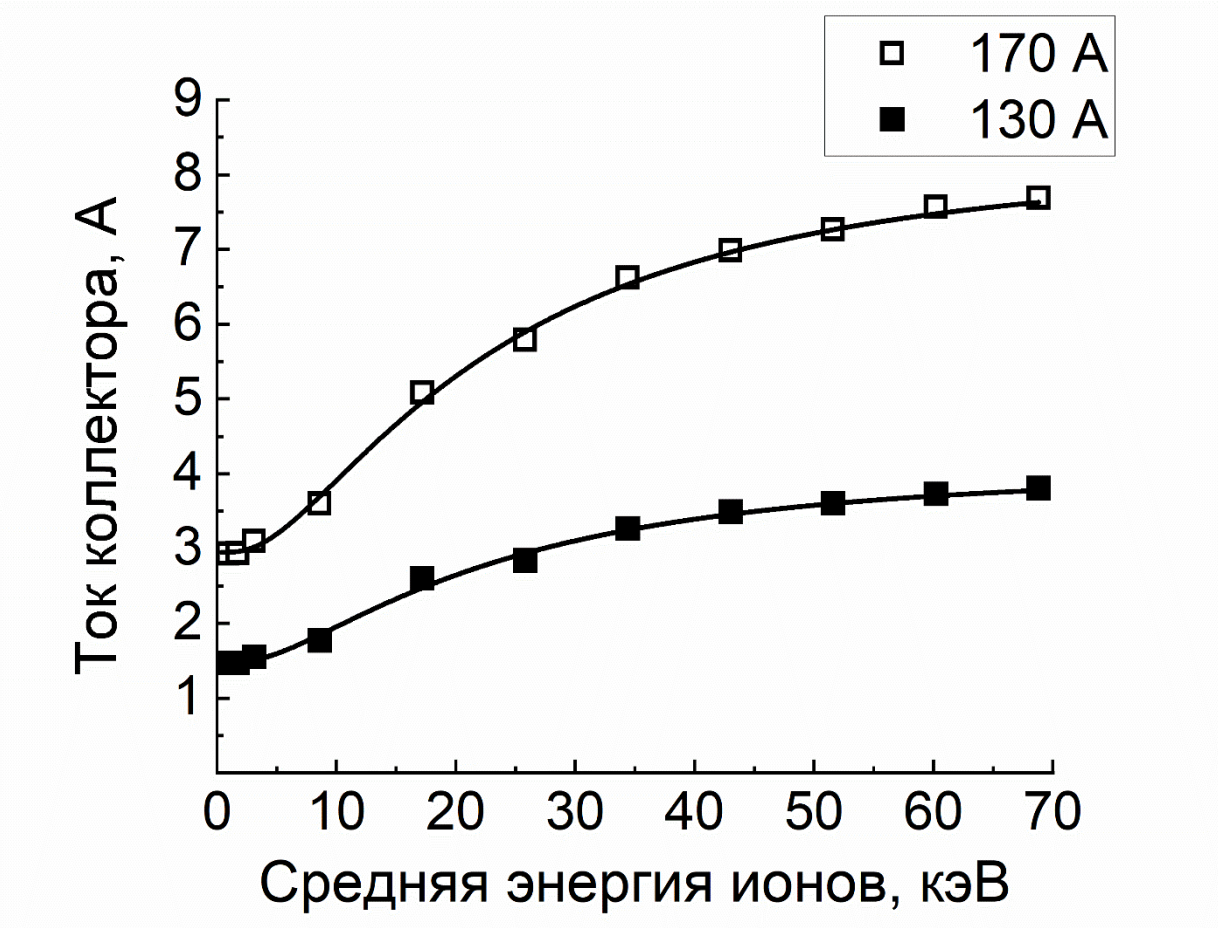
170 A
130 A
Ток коллектора, А
1
2
3
4
5
6
7
8
9
0
10
20
30
40
50
60
70
Средняя энергия ионов, кэВ

Fig. 11.

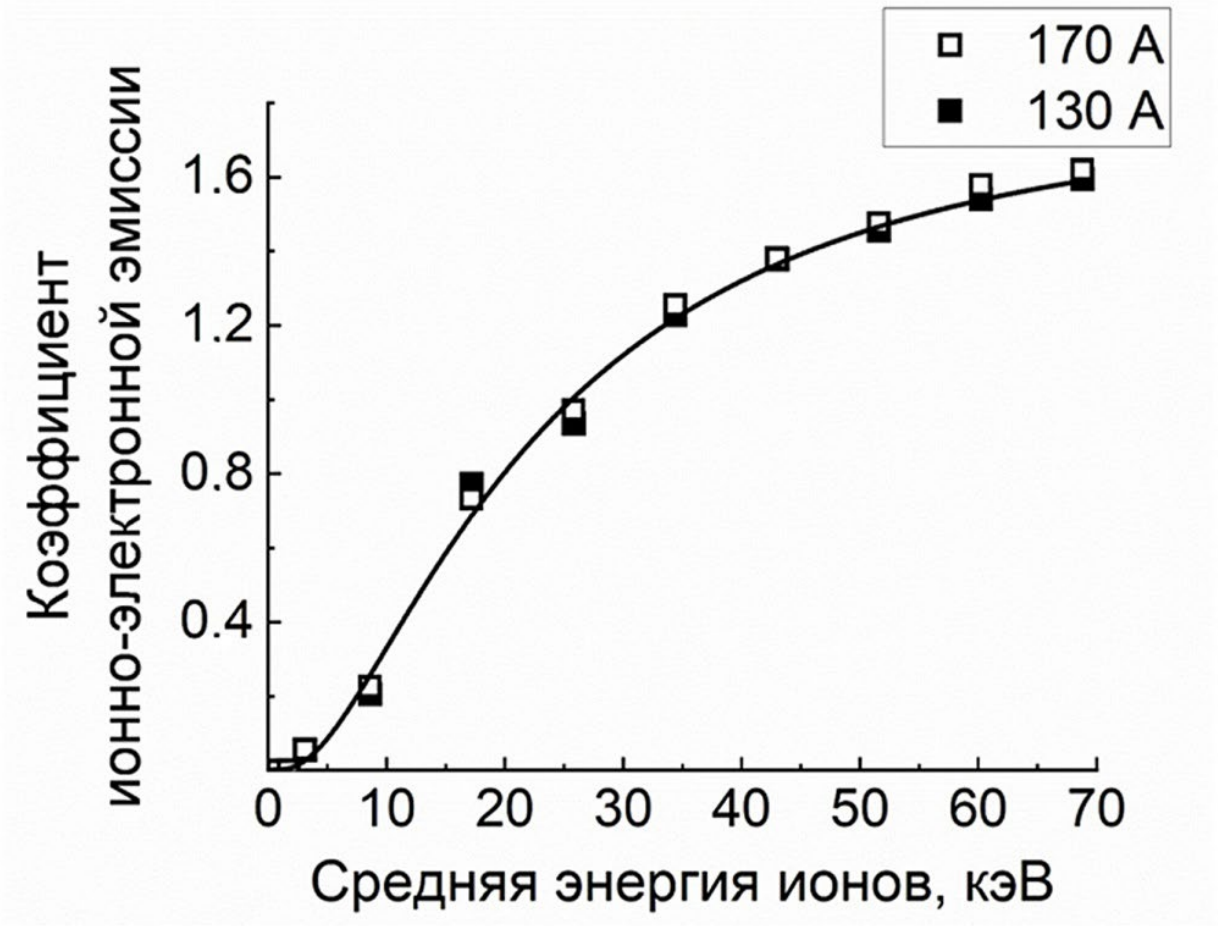
170 A
130 A
Коэффициент ионно-электронной эмиссии
1.6
1.2
0.8
0.4
0
10
20
30
40
50
60
70
Средняя энергия ионов, кэВ

Fig. 12.